

Influence of PWHT on Toughness of High Chromium and Nickel Containing Martensitic Stainless Steel Weld Metals

M. DIVYA, CHITTA RANJAN DAS, S. MAHADEVAN, S.K. ALBERT, R. PANDIAN, SUJOY KUMAR KAR, A.K. BHADURI, and T. JAYAKUMAR

Commonly used 12.5Cr-5Ni consumable specified for welding of martensitic stainless steels is compared with newly designed 14.5Cr-5Ni consumable in terms of their suitability for repair welding of 410 and 414 stainless steels by gas tungsten arc welding process. Changes in microstructure and austenite evolution were investigated using optical, scanning electron microscopy, X-ray diffraction techniques and Thermo-Calc studies. Microstructure of as-welded 12.5Cr-5Ni weld metal revealed only lath martensite, whereas as-welded 14.5Cr-5Ni weld metal revealed delta-ferrite, retained austenite, and lath martensite. Toughness value of as-welded 12.5Cr-5Ni weld metal is found to be significantly higher (216 J) than that of the 14.5Cr-5Ni weld metal (15 J). The welds were subjected to different PWHTs: one at 923 K (650 °C) for 1, 2, 4 hours (single-stage PWHT) and another one at 923 K (650 °C)/4 h followed by 873 K (600 °C)/2 h or 873 K (600 °C)/4 h (two-stage heat treatment). Hardness and impact toughness of the weld metals were measured for these weld metals and correlated with the microstructure. The study demonstrates the importance of avoiding formation of delta-ferrite in the weld metal.

DOI: 10.1007/s11661-015-2847-y

© The Minerals, Metals & Materials Society and ASM International 2015

I. INTRODUCTION

LOW carbon martensitic stainless steels containing 0.03 wt pct carbon and 5.0 wt pct nickel are widely used for many turbine components in power plants because of their good toughness and strength.^[1–5] Presently, these steels find wide applications in oil and gas industries in place of expensive duplex stainless steels due to their good corrosion resistance and weldability.^[1,4,6] Although these steels are weldable, commercially available consumables for welding are not exactly matching in composition with the base metal. Hence, often austenitic stainless steel filler wires are considered for welding, especially in the case of repair welding for which it is difficult to meet the requirements of post-weld heat treatment (PWHT) recommended for welding with martensitic stainless steel consumables. Repair welding with 410 filler wire is difficult not only because of the challenge in achieving the required temperature [1008 K (735 °C)] during *in situ* PWHT but also in obtaining desired toughness in the weld metal. *In situ* PWHT of repaired turbine components made from this class of steels at a high temperature is an integrity concern, as nearby components will get heated up. Further, in spite of this high temperature PWHT, it

is reported that the toughness of 410 weld metal cannot be enhanced beyond 25 to 30 J.^[7]

AISI 414 SS, a martensitic stainless steel is a modified version of AISI 410 SS with addition of Ni and Mo to it. Microstructure of this steel in normalized and tempered (N&T) conditions consists of lath martensite and retained austenite.^[1–5] Two-stage tempering is employed to achieve suitable strength, toughness, and corrosion resistance in these steels.^[1,2,8] Similarly, the matching welding consumables used for welding this steel E/ER 410NiMo requires two-stage PWHT in the range of ~ 853 K to 953 K (580 °C to 680 °C) to restore corrosion resistance and toughness.^[2,6,9,10] In the first stage, the material is heated to a temperature just above the A_{c1} transformation temperature and cooled to room temperature, and in the second stage, the same material is heated to a temperature just below the A_{c1} transformation temperature and cooled to room temperature.^[6] Studies on weld joints of this steel showed an increase in volume fraction of retained austenite during PWHT which in turn leads to an increase in the toughness.^[1,3,8] The higher volume fraction of retained austenite observed in second stage of heat treatment (PWHT at a lower temperature) was attributed to be the cause for the improvement in toughness; however, the mechanism by which this increase takes place is not yet understood clearly. Song *et al.*^[10] reported that volume fraction of retained austenite is lower after first stage PWHT at higher temperature than that after second stage PWHT at lower temperature and this is correlated to formation of austenite at the $M_{23}C_6$ precipitate/matrix interface.

In high Cr steels, the presence of delta-ferrite is known to impair formability, toughness, and corrosion properties.^[11–15] Detrimental effect of this phase on

M. DIVYA and R. PANDIAN, SO/Ds, CHITTA RANJAN DAS and S. MAHADEVAN, SO/Fs, S.K. ALBERT, Head, MTD, A.K. BHADURI, AD, MDTG, and T. JAYAKUMAR, Director, MMG, are with Indira Gandhi Centre for Atomic Research, Kalpakkam 603102, Tamil Nadu, India. Contact e-mail: chitta@igcar.gov.in SUJOY KUMAR KAR, Professor, is with the Metallurgical and Materials Engineering, Indian Institute of Technology, Kharagpur, India.

Manuscript submitted May 27, 2014.

Article published online March 21, 2015

creep in 9-12Cr steels (like grade 91, 92, *etc.*) is reported widely.^[16,17] At high temperatures, delta-ferrite transforms to sigma phase and causes degradation in mechanical properties.^[18] This phase also raises the ductile brittle transition temperature (DBTT) of 9-12Cr steels.^[4,15] Anderko *et al.*^[16] reported lower DBTT for 11Cr steel containing 0.5 pct volume fraction of delta-ferrite than for delta-ferrite-free 10Cr steel. Although the influence of delta-ferrite on the mechanical properties has been studied extensively, no relationship has been established between volume fraction of delta-ferrite and toughness. According to one school of thought, cohesive strength between delta-ferrite and matrix phase is low and this is the reason for poor toughness of the weld metal that contains delta-ferrite.^[19,20] Another school of thought is that delta-ferrite, being a soft phase, improves toughness.^[6] The complex microstructure of high Cr steel weld metal could be one of the reasons for these disagreements.^[21]

Therefore, a systematic study is required to understand the role of delta-ferrite in high chromium and nickel containing weld metal under different PWHT conditions. It is also necessary to understand the role of retained austenite in such high chromium and nickel martensitic stainless steels weld metals. Hence, a detailed study comparing the toughness and microstructure of the weld metals containing retained austenite with delta-ferrite and another without delta-ferrite would enhance the present understanding of various weld metals in use. This is the primary objective of the present investigation.

II. EXPERIMENTAL

Two weld pads were prepared by gas tungsten arc welding (GTAW) process with 12Cr martensitic stainless steel (AISI 410) plates of 12-mm thickness using 12.5Cr-5Ni (ER410NiMo) and 14.5Cr-5Ni filler wires. A total of 17 weld passes were used to complete the welding for each weld pad. Newly designated filler wire of composition 14.5Cr-5Ni was prepared by spot welding of ER 410 filler wire of 2 mm diameter and ER 16-8-2 wire of 1.5 mm diameter along their length at regular interval and used as a single wire during welding. This combination was chosen to closely match the chemical composition of turbine blade material. Welding was carried out using current and voltage of 100 A and 10 V, respectively, at a welding speed of 0.88 mm s⁻¹. For both the weld pads, preheat, interpass, and post-heating temperatures were maintained at 500 K to 523 K (227 °C to 250 °C). Thereafter, weld pads were subjected to radiographic examination and

subsequently they were sliced into 12 × 12 × 57 mm³ specimen blanks ensuring that weld metal is at the center of the blank. These sliced specimen blanks were subjected to PWHT at different temperatures and durations to carry out microstructural examination and for evaluating hardness and impact toughness. It may be worth mentioning that the Ac₁ transformation temperatures of 12.5Cr-5.5Ni and 14.5Cr-5.5Ni are 903 K and 913 K (630 °C), respectively, estimated from the hardness vs tempering temperature plot.^[6] All the heat-treated specimens are designated as detailed in Table I.

Chemical composition of the weld metals was analyzed using optical emission spectrometry. Hardness of the two weld metals both in the as-welded and after different PWHT conditions was measured at room temperature using Vicker's hardness tester at 10 kg load and 15 seconds loading time. Full size Charpy-V impact specimens of 55 × 10 × 10 mm³ were prepared from the sliced specimen blanks, as per ASTM E23 with V notch along the welding direction. Impact tests were carried out both in the as-welded and after PWHT conditions at room temperature using an instrumented impact test machine of capacity 358 J. Instrumented tests were performed to obtain load-displacement plots.

For microstructural observations, metallographic specimens were prepared from the heat-treated weldments. These specimens were metallographically polished and etched using Vilella's reagent. The etched specimens were then observed under optical microscope and scanning electron microscope (SEM). SEM make of CamScan 3200, UK, and Ultra-high resolution FE-SEM (Model SPURA 55), Zeiss were used for microstructural and fractographic observation. Energy dispersive spectroscopic (EDS) attached with FESEM was used for analyzing localized changes in microchemistry caused by the heat treatment. Spectra were collected for 2 minutes to get 1000 to 20,000 counts using 20 kV. For EBSD studies, specimens were mechanically polished in a polishing disk at a low rotation speed of 100 rpm during each stage to minimize the mechanical deformation. Subsequently, they were electrochemically polished at 10 V for 10 to 15 seconds in a solution of 20 mL of perchloric acid and 80 mL of methanol maintained at sub-zero temperature. EBSD studies on the specimens were made using FESEM equipped with an EBSD system operating at an accelerating voltage of 40 kV with the sample tilted at 70 deg with respect to horizontal axis. The area selected for EBSD analysis was 100 × 100 μm² at 400× magnification with a scan step size of 0.5 μm. Two structure files of bcc (α-Fe) and fcc (γ-Fe, austenite) were used to

Table I. PWHT Conditions of the Two Weld Metals Used and Their Designations

Sample Designation	As-welded	PWHT Conditions				
		923 K (650 °C)/1 h	923 K (650 °C)/2 h	923 K (650 °C)/4 h	923 K (650 °C)/4 h + 873 K (600 °C)/2 h	923 K (650 °C)/4 h + 873 K (600 °C)/4 h
12.5Cr-5Ni weld metal	AW-1	1A	1B	1C	1D	1E
14.5Cr-5Ni weld metal	AW-2	2A	2B	2C	2D	2E

generate EBSD results. These experiments were carried out on 12.5Cr-5Ni weld metal only to understand the influence of PWHT on grain boundary character distributions in this weld metal.

X-ray diffraction (XRD) measurements were carried out on all the specimens investigated in this study using Rigaku strainflex MSF-2M X-ray diffractometer with Cr-K_α radiation for retained austenite analysis. The XRD profiles of all the specimens were recorded in the angular range of 121 to 133 and 150 to 162 deg for recording the peaks from austenitic and ferritic phases, respectively. The peaks were separated using a Voigt function and a suitable background. The volume fraction of austenite phase was determined by direct comparison of integrated intensities of the (220) planes corresponding to the austenitic phase and the intensities of the (211) planes corresponding to the ferritic phase.^[22] The integrated intensities of the Voigt peaks were used for estimating the volume fraction of austenite using the code available at materials Algorithm project at University of Cambridge.^[23] Phase balance diagrams for both of these weld metals were generated using Thermo-Calc software (TCC version S) and Thermodynamic database module TCFE6.^[24]

III. RESULTS

A. Chemical Composition

Chemical composition of the weld metals is given in Table II. It can be seen from Table II that the composition of both weld metals are similar except for the composition of C, Cr, Mn, and Mo. 12.5Cr-5Ni and 14.5Cr-5Ni weld metals contain 0.02 and 0.05 wt pct carbon, respectively. 14.5Cr-5Ni weld metal contains 0.5 wt pct higher Mo than that of 12.5Cr-5Ni weld metal. Chromium and nickel equivalents (Cr_{eq} and Ni_{eq}) were estimated from the composition using empirical equations given by Balmforth diagram^[12] and the same are tabulated in Table II along with composition. It is clear from the table that Cr_{eq} and Ni_{eq} values are higher for 14.5Cr-5Ni weld metal than 12.5Cr-5Ni weld metal

suggesting to the possibility of 14.5Cr-5Ni weld metal to have some delta-ferrite under similar welding condition.

B. Hardness and Toughness of Weld Metal

Hardness and toughness values obtained using procedures indicated in Section II for all the specimens are tabulated in Table III. It is clear that, in the as-welded condition, the hardness of AW-1 weld metal (341 VHN) is lower than that of AW-2 weld metal (400 VHN) and after PWHT at 923 K (650 °C) for 1h, reduction in hardness is less for 12.5Cr-5Ni steel than that observed for 14.5Cr-5Ni steel. However, with increase in holding time at this temperature beyond 1 hour, further change in hardness is only marginal for both the weld metals. After 4 hours of first stage PWHT, followed by second stage PWHT at a lower temperature of 873 K (600 °C) for 2 hours, the hardness values of both the weld metals decreased further. However, on increasing the holding time to 4 hours at lower temperature (second stage), hardness of both the weld metals increased marginally. These results are in contrast to our common understanding of change in material behavior with variation in PWHT/tempering temperature and are discussed later.^[25]

The impact toughness of 12.5Cr-5Ni weld metal in as-welded condition is 216 J which is significantly higher than the 15 J obtained in 14.5Cr-5Ni weld metal in the same condition. This high value of toughness in as-welded condition obtained for 12.5Cr-5Ni steel is not commonly observed in martensitic stainless steel weld metals. Although a decrease in hardness value accompanied by an increase in toughness value is expected after PWHT, it is observed that the toughness value of 12.5Cr-5Ni weld metal remained similar to that of as-welded condition after PWHT at 923 K (650 °C) up to 4 hours. This observation is attributed to the similar lath martensite morphology and similar volume fraction of retained austenite as first stage PWHT has been carried out just above A_{c1} temperature. Further, PWHT at 923 K (650 °C) does not seem to improve the toughness, though a decrease in hardness is observed.

Table II. Chemical Composition of the Weld Metals in Weight Percent

Elements	C	Cr	Ni	Mn	Mo	P	S	Si	Cr _{eq}	Ni _{eq}
12.5Cr-5Ni	0.02	12.50	5.00	0.45	0.50	0.02	0.04	0.4	13.56	5.7
14.5Cr-5Ni	0.05	14.50	5.00	0.80	1.00	0.03	0.01	0.26	16.89	6.75

Table III. Hardness and Toughness of the Weld Metals After Various PWHTs

Sample ID of Series-1	Hardness (VHN)	Charpy Impact Toughness (J)	Sample ID of Series-2	Hardness (VHN)	Charpy Impact Toughness (J)
AW-1	341 ± 4	216 ± 5	AW-2	400 ± 35	15 ± 3
1A	300 ± 5	215 ± 6	2A	298 ± 5	64 ± 2
1B	304 ± 3	213 ± 2	2B	294 ± 1	66 ± 4
1C	299 ± 2	224 ± 8	2C	302 ± 1	63 ± 3
1D	270 ± 2	178 ± 4	2D	289 ± 5	89 ± 9
1E	307 ± 5	202 ± 8	2E	303 ± 2	100 ± 7

In contrast, PWHT at this temperature (for 2A condition) for an hour increased the toughness of 14.5Cr-5Ni weld metal to 64 J with corresponding decrease in hardness to 298 VHN from the as-welded hardness value. Interestingly, with increase in hold time at this PWHT temperature, the toughness and hardness values remained similar as seen in the case of 12.5Cr-5Ni weld metal.

In 12.5Cr-5Ni weld metal, the second stage heat treatment at 873 K (600 °C) for 2 hours (1D condition) reduced the hardness and toughness values to 270 VHN and 178 J from 299 VHN to 224 J, respectively. This relative decrease in hardness and toughness values is not a common observation. On increasing the hold time to 4 hours at this temperature, the impact toughness and hardness values increased to 202 J and 307 VHN, respectively. Concurrent increase in hardness and toughness is not commonly observed in ferritic/martensitic class of steels and these call for better understanding of microstructural evolution during PWHT. However, in 14.5Cr-5Ni weld metal, the second stage PWHT at 873 K (600 °C) for 2 and 4 hours, increased the toughness value to 89 and 100 J, respectively, and the observed changes are on expected lines. But variation in hardness remains similar to that observed in 12.5Cr-5Ni weld metal. In short, it can be stated that high as-welded toughness in 12.5Cr-5Ni steel weld metal did not change significantly after first stage of PWHT, but shows a relative decrease after the two stages of PWHT. For 14.5Cr-5Ni weld metal, the as-welded toughness was very low and it increased significantly after single-stage heat treatment which increased further after the second stage heat treatment.

C. Analysis of Instrumented Charpy Impact Test Data

Load vs time data obtained from the instrument were processed and converted to Load vs displacement plot. Load-displacement plots of 12.5Cr-5Ni and 14.5Cr-5Ni weld metals at the end of first stage (1C and 2C) and second stage PWHTs (1E and 2E) are shown in Figure 1. Area under the curve is a measure of tough-

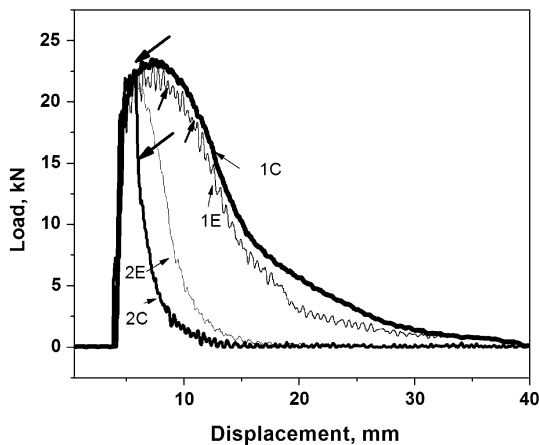


Fig. 1—Typical load-displacement plots for 12.5Cr-5Ni and 14.5Cr-5Ni weld metals.

ness of the material. In 12.5Cr-5Ni weld metal, the area under the curve after second stage PWHT is lower than that of the first stage PWHT. This is consistent with reduced toughness of this weld metal as shown in Table III. Interestingly, the number of serrations observed in the load-displacement plot has increased significantly at the end of second stage. For 14.5Cr-5Ni weld metal, the second stage heat treatment enhanced the area under the curve with decrease in peak load and marginal increase in number of serrations. These observations are consistent with the changes in toughness values. The figure also reveals that for 14.5Cr-5Ni weld metal (at end of first stage—923 K (650 °C)/4 h) a sudden drop in load from the peak value of 21.6 to 14.8 kN (marked in the figure) is observed which is an indication of initiation of an unstable crack.

D. Microstructures

Optical photomicrographs of top, middle, and root regions of 1C and 2C weld metals after 923 K (650 °C)/4 h heat treatment are shown in Figure 2. The microstructures of 12.5Cr-5Ni weld metal shown in Figures 2(a) through (c) reveal tempered lath martensite wherein the prior austenite grain boundaries are clearly evident. The prior austenite grain size in the middle and root regions is finer than the top region of the weldment. These observed variations in the prior austenite grain size are attributed to the multiple thermal cycles experienced by the multipass weld metal during subsequent fill passes.

The microstructures of top, middle, and root regions of 14.5Cr-5Ni weld metal are shown in Figures 2(d) through (f) which consist of both lath martensite and delta-ferrite. The area fraction of delta-ferrite estimated using image analysis software (Image J) from the top, middle, and root regions of 2C weld metal is 35, 5.4, and 0.5 pct, respectively. The morphology of delta-ferrite changes from the top to root with highly interconnected network at the top and isolated delta-ferrite at the root region of the weld joint. The variation in the area fraction of delta-ferrite is attributed to transformation of delta-ferrite formed in the initial layer during deposition of the subsequent layers. On subsequent deposition of the weld metal, this delta-ferrite transforms to austenite during the heating part of the thermal cycle and this freshly formed austenite transforms back to martensite during the cooling part.

E. SEM Micrographs

Typical electron micrographs of specimens 1A, 1C, 1D, and 1E along with 2A, 2C, 2D, and 2E taken at 45 deg inclinations are shown in Figures 3(a) through (d) and (e) through (h), respectively. It is to be noted that Figures 3(e) through (h) are taken from regions free of delta-ferrite for better understanding of matrix features. The morphological differences were not clear in the micrographs taken at normal incidence necessitating 45 deg tilt. The morphology of lath martensite after single-stage heat treatment remains similar in both the weld

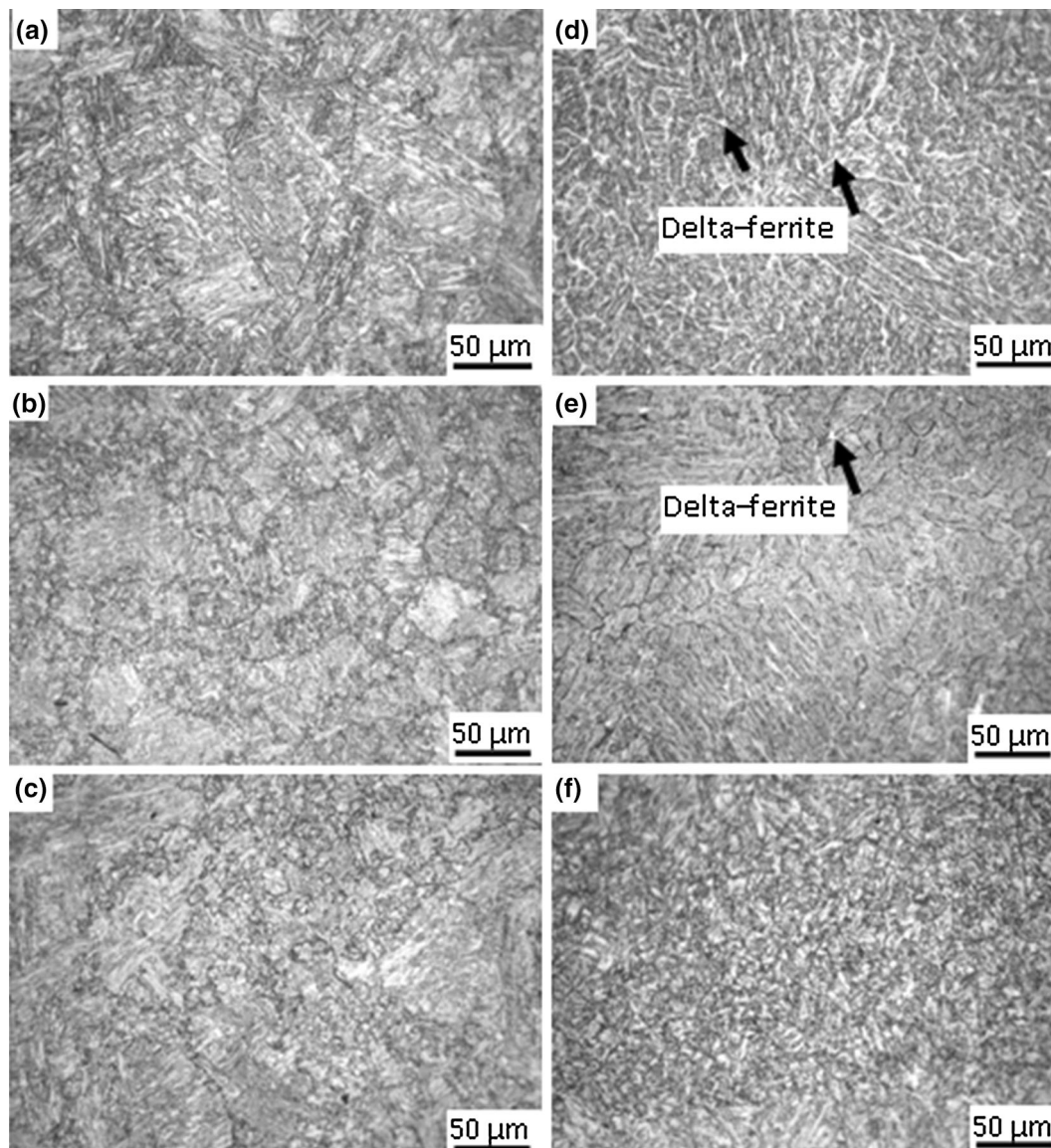


Fig. 2—Photomicrographs of top, middle, and root region of specimen 1C (*a* through *c*) and 2C (*d* through *f*).

metals. Similar observations were recorded in as-welded condition. The microstructures of second stage heat-treated specimens shown in Figures 3(c), (d), (g), and (h) are distinctly different from that of the first stage heat-treated specimens. From Figure 3(c), it is evident that second phase (bright in contrast) is present at the lath martensite boundaries. On the other hand, the secondary electron (SE) image of 14.5Cr-5Ni weld metal shown in Figure 3(g) reveals that the bright second phase having morphology different from those observed in 12.5Cr-5Ni weld metal being present at the lath boundaries. At the end of second stage heat treatment, the microstructural features of matrix phase are finer in 1E (Figure 3(d)) and 2E (Figure 3(h)) than in 1D and 2D.

In order to understand the chemistry of brighter regions (those could be retained austenite or $M_{23}C_6$ precipitate) seen in the micrographs, EDS spectra were

obtained in normal incidence. The EDS spectrum shown in Figures 4(a) and (b) is taken from the brighter region marked with black square and dark region marked with circle of 12.5Cr-5Ni weld metal (specimen 1E) in Figure 4(b). An approximate estimation of the composition of the white region from the EDS spectrum indicates that these regions contain more nickel than the matrix. Higher Ni content is 10 wt pct in this bright region than the average of 4.5 wt pct is attributed to the austenite phase. Higher Ni content than the matrix phase is sufficient to bring down the localized martensitic start (M_s) and finish (M_f) temperatures of brighter regions below sub-zero. Hence, this will remain untransformed after cooling and was confirmed by XRD analysis and is presented in the following Section III-G.

Similarly, a typical EDS spectrum shown in Figure 5(a) from the region marked with square in Figure 5(b) of 14.5Cr-5Ni weld metal (specimen 2E)

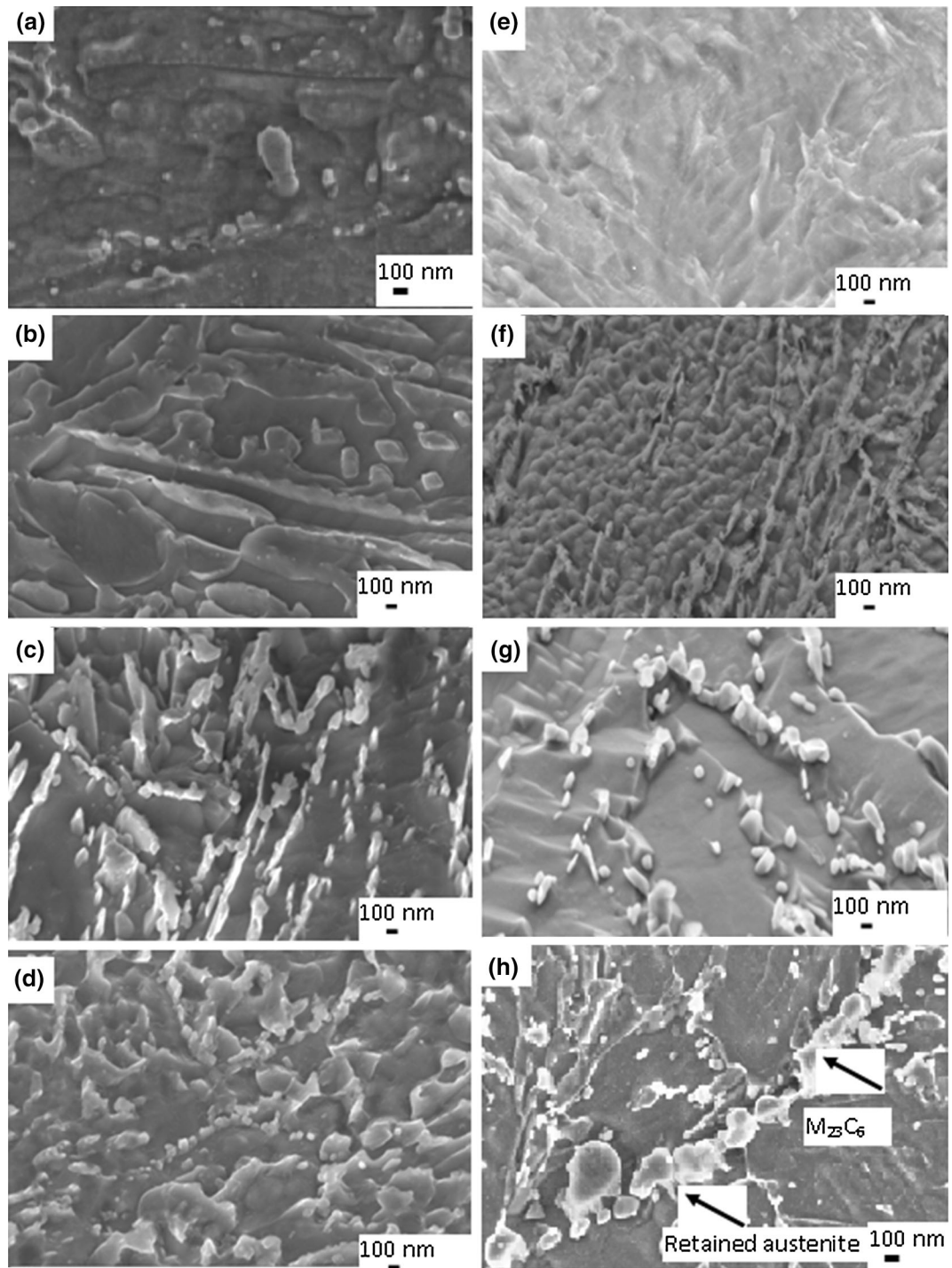


Fig. 3—Photomicrographs of 12.5Cr-5.5 Ni weld metal under different heat treatment conditions (a through d) and 14.5Cr-5.5 Ni weld metal under different heat treatment conditions (e through h).

shows that these regions are rich in Cr, Fe, and lean with Ni which is inferred as regions of delta-ferrite. EDS taken from the brightest regions present at the matrix/delta-ferrite interface (marked with circle) shows the presence of Cr and Fe and is lean in nickel leading to infer that these are $M_{23}C_6$ carbides. EDS taken at the precipitate-matrix interface was found to be rich in Ni and this is marked as austenite.

F. EBSD Results

In order to understand the influence of PWHT temperature and durations on grain boundary character distribution, electron back-scattered diffraction (EBSD) studies on 12.5Cr-5Ni weld metal in different heat-treated conditions were carried out. Inverse pole figure maps (IPF) of the weld metal obtained from the cap region of 1D and 1E weld metal specimens are shown in

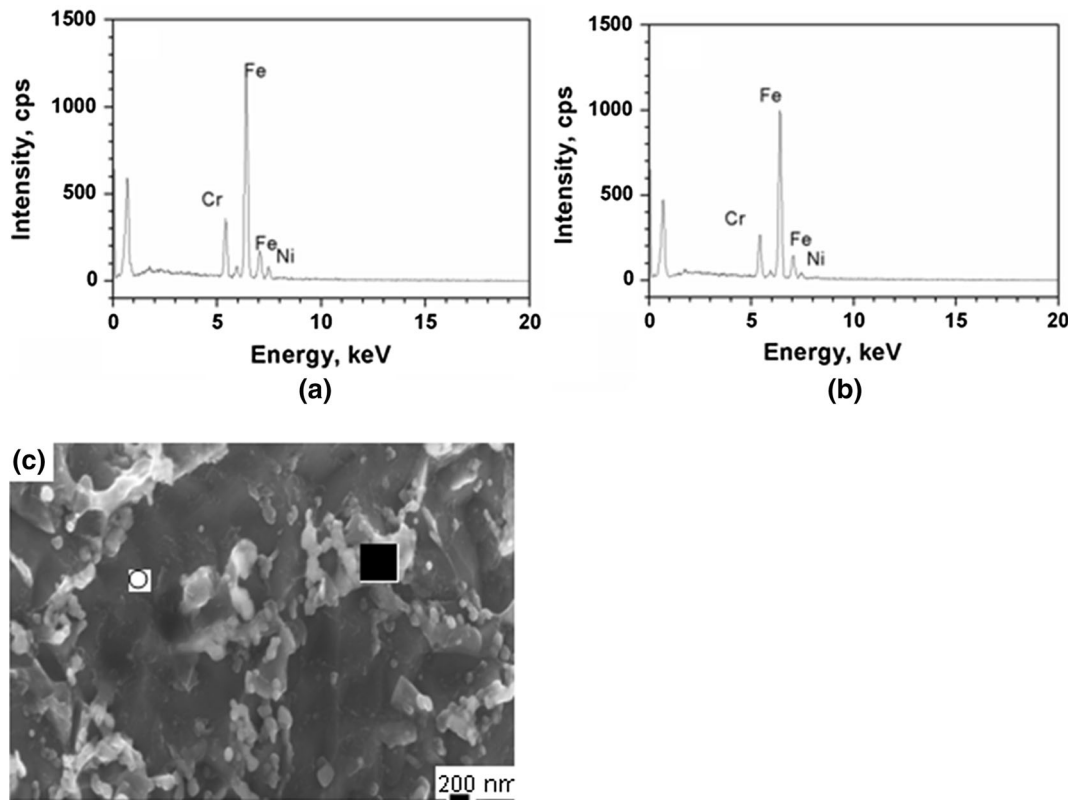


Fig. 4—(a) EDS obtained from the bright region marked with black square on the SE image, (b) EDS obtained from the matrix marked with circle on the image, and (c) SE image of 1E specimen.

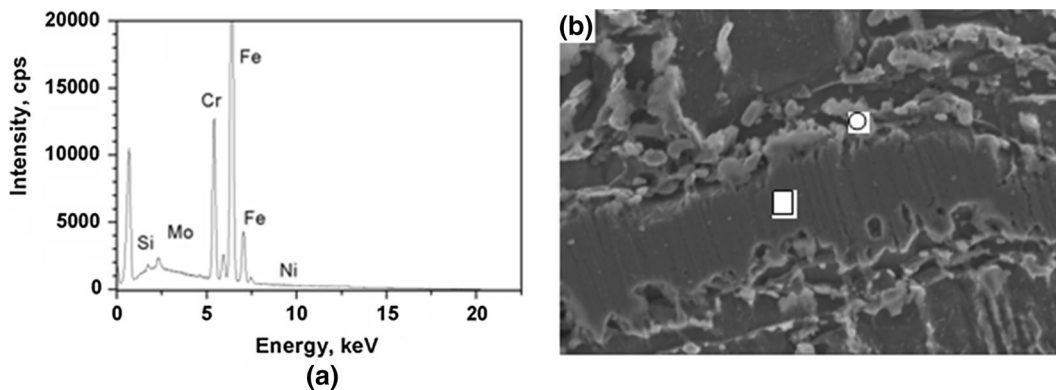


Fig. 5—(a) EDS obtained from the white region present at the lath martensite interface and (b) SE image of that region obtained from 2E weld metal.

Figures 6(a) and (b), which show coarser features in 1D compared to 1E. This feature is similar to that observed in Figure 3(c). Figure 7 shows the boundary line fraction against misorientation angle for this 12Cr-5Ni weld metal in different heat-treated conditions.

G. X-ray Diffraction Studies

In order to estimate the volume fraction of retained austenite in these materials, XRD measurements were carried out as per the procedures mentioned in Section II. Typical XRD peaks of a few samples in 1 and 2 series

are shown in Figures 8(a) and (b) with the legends identifying the samples. The peaks from the matrix (α -(211)) and austenite (γ -(220)) are indexed. The XRD measurements in 12.5Cr-5Ni weld metals in the as-welded state and after first stage heat treatment did not reveal significant volume of retained austenite. Nevertheless, prominent austenite peaks were observed after the second stage of heat treatment at 873 K (600 °C) and the volume fraction was estimated as 13 pct. On the other hand, the volume fraction of retained austenite in the as-welded 14.5Cr-5Ni weld metal is found to be 10 pct. The presence of austenite in the as-welded

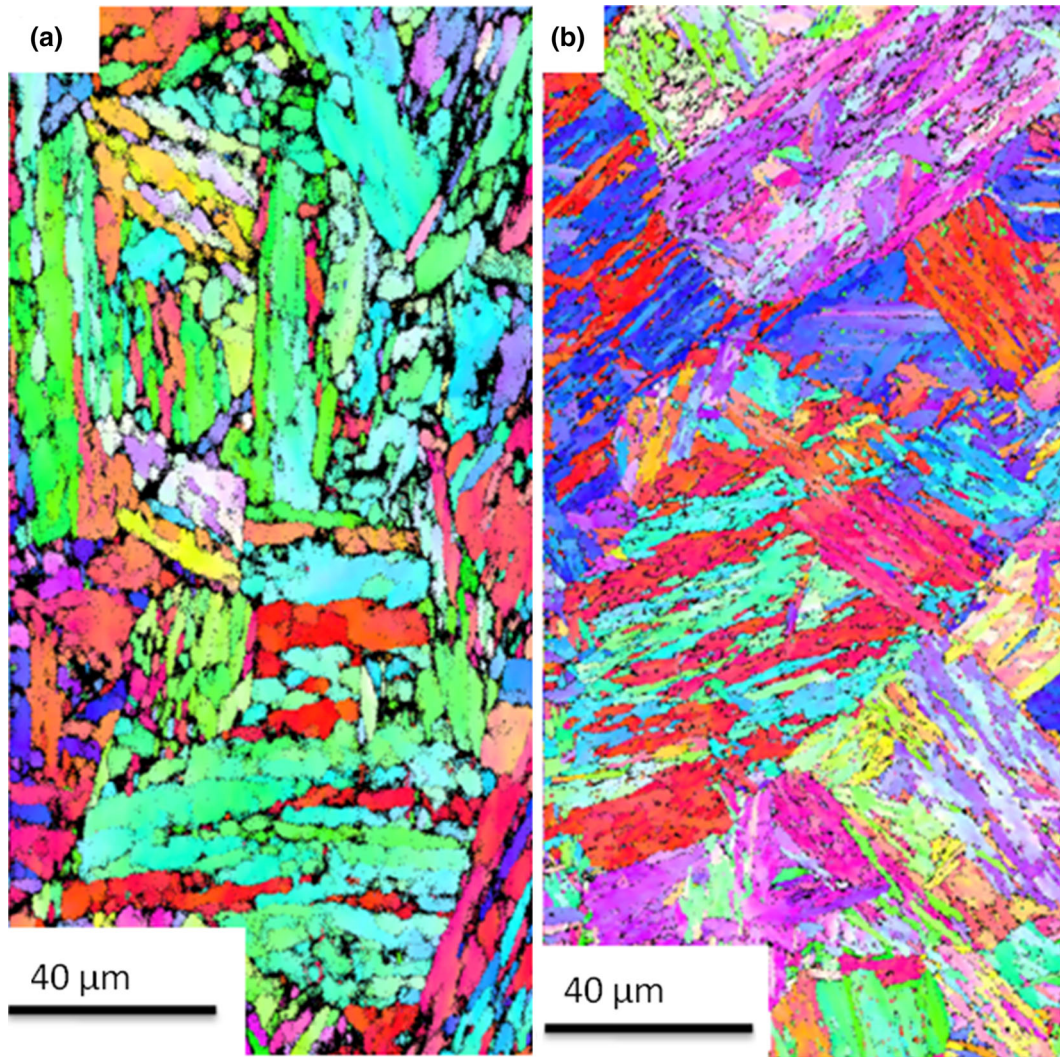


Fig. 6—Inverse pole figure map obtained from the same location of (a) 1D and (b) 1E specimens.

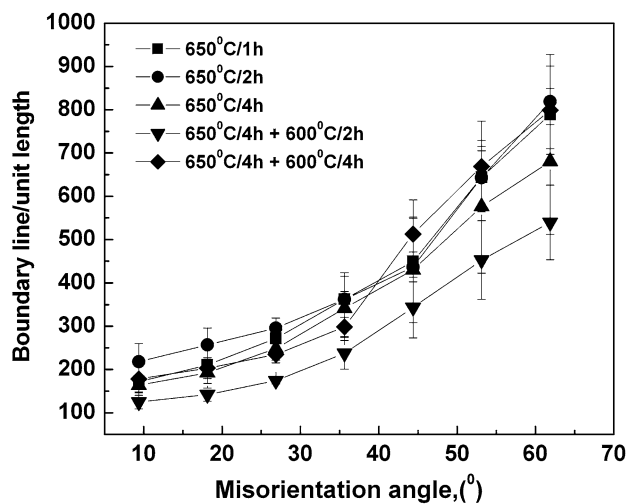


Fig. 7—Boundary line length for martensite phase in 12.5Cr-5Ni weld metals.

14.5Cr-5Ni weld metal is attributed to the presence of significant amount of delta-ferrite which rejects austenite stabilizing elements during cooling and enriches the matrix. After first stage heat treatment, the amount of austenite remains similar. However, after second stage PWHT, the volume fraction of retained austenite increased marginally to 15 pct.

H. Fractography

All the fractured surfaces of Charpy-V impact specimens were observed under SEM. Fractographs of as-welded 12.5Cr-5Ni and 14.5Cr-5Ni weld metals are shown in Figures 9(a) and (b), respectively. Typical ductile dimples are seen in the fractograph of AW-1 specimen (Figure 9(a)), whereas a quasi-cleavage fracture surface is seen in AW-2 specimen (Figure 9(b)), which are in agreement with the respective Charpy impact toughness values given in Table III. The fractographs of 12.5Cr-5Ni weld metal after first stage heat treatment do not show much change from the fractograph of as-welded specimens and this is in consistent

with similar Charpy impact values obtained for this weld metal in both the conditions. The fractographs of 1D and 1E specimens are shown in Figures 10(a) and (b), respectively. This change in morphology of fractographs in Figures 10(a) and (b) is in line with the micrographs shown in Figures 3(c) and (d). In 1D

condition, fractograph reveals mixture of finer dimples and cleavage facets, while dimples are more uniform in 1E condition. This is in line with the lower toughness observed under this condition. Although at this point of time it is not possible to explain why such a mixed mode failure occurs in 1D condition, it is apparent from this that the morphology of austenite is different in this condition compared to 1E condition.

Figures 11(a) and (b) show the fractographs of 14.5Cr-5Ni weld metal in 2C and 2E conditions. The fracture surface at the end of first stage heat treatment (sample 2C) shows de-cohesion of the delta-ferrite from the matrix as shown in Figure 11(a), suggesting lower interfacial energy.^[26] It may be noted that the austenite fraction remains similar in as-welded and after first stage heat treatment. De-cohesion of delta-ferrite from the matrix is directly linked to the sharp fall in peak load as shown in Figure 1. But with increase in PWHT durations during second stage heat treatment, austenite volume fraction increases. In this condition, it is quite possible that interfacial strength has increased compared to the strength of delta-ferrite resulting fracture of delta-ferrite as shown in Figure 11(a).

IV. DISCUSSION

From the results presented in Section III, it is clear that the composition of both weld metals is similar except for the concentrations of C, Cr, Mn, and Mo which are relatively higher in AW-2 weld metal than in AW-1. In addition to minor compositional differences between the two weld metals, AW-2 weld metal has 10 pct retained austenite and 35 pct delta-ferrite in lath martensitic matrix. On the other hand, AW-1 weld metal has only very low volume fraction (below detection limit) of retained austenite in the martensitic matrix and it was free from the delta-ferrite. These differences in microstructure are also reflected in fairly large variations in the toughness of the two weld metals in the as-welded condition, after single stage and after two stage PWHT. Possible reasons for these variations in microstructure and properties of these two weld metals are discussed here based on the results obtained.

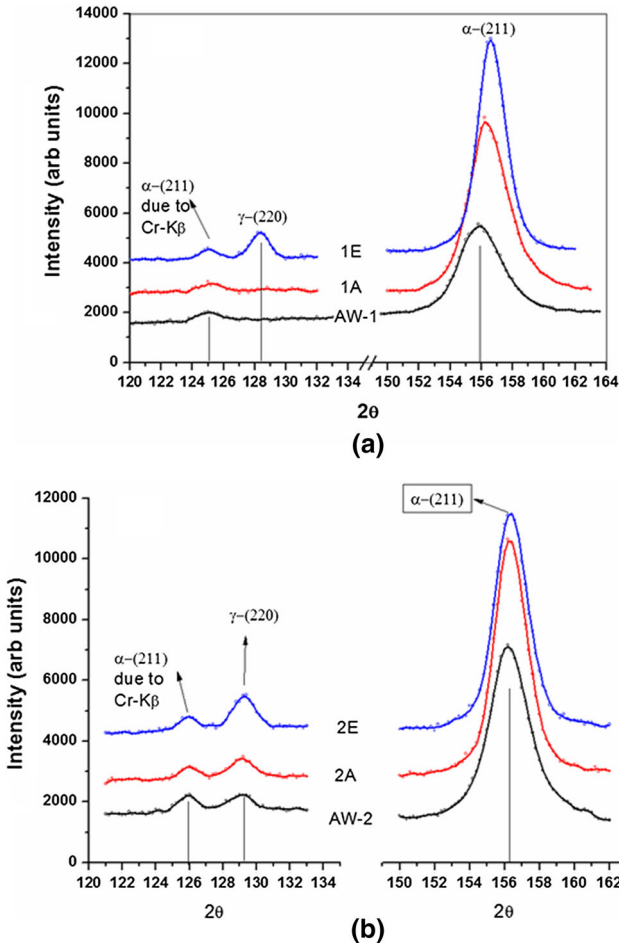


Fig. 8—(a, b) X-ray diffractograms of 12.5Cr-5Ni and 14.5Cr-5Ni weld metals under various heat treatment conditions with appropriate legends.

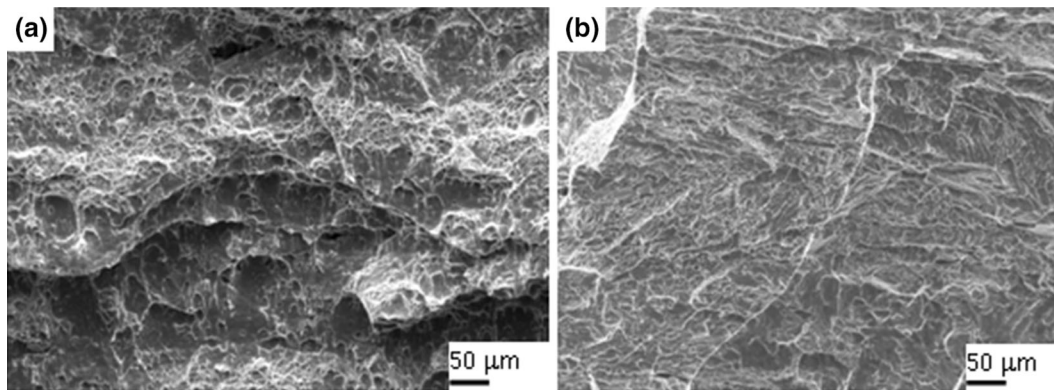


Fig. 9—Fractographs of 12.5Cr-5Ni and 14.5Cr-5Ni weldments in as-welded condition.

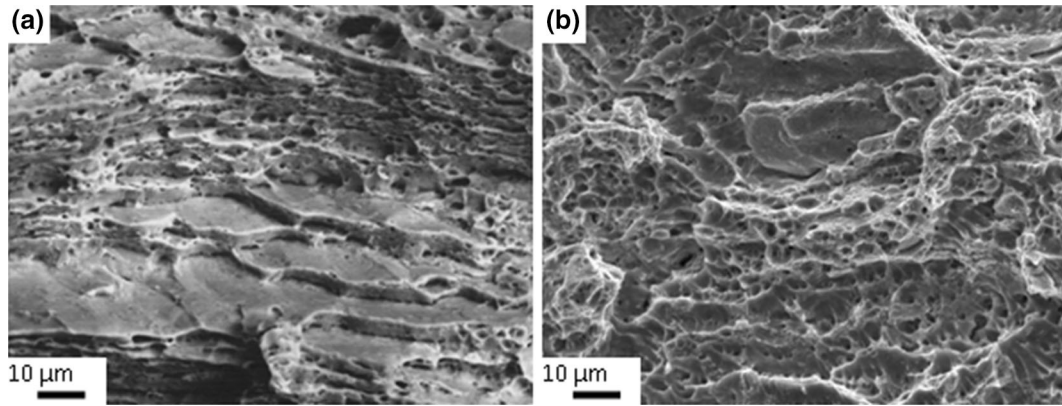


Fig. 10—Fractograph of 12.5Cr-5Ni weld metal in (a) 1D and (b) 1E conditions.

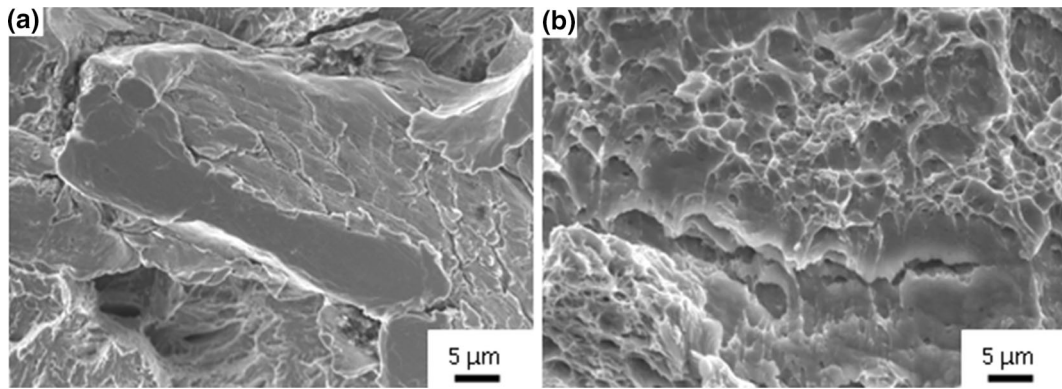


Fig. 11—Fractographs of 14.5Cr-5Ni weld metal in (a) 2C and (b) 2E conditions.

A. Effect of Composition on Phase Balance

In order to understand the comparative differences in the microstructure of both the weld metals after PWHT, phase stability diagram (amount of phases vs temperature) and Scheil solidification sequence for both the alloys have been calculated and plotted using Thermo-Calc software and TCFE6 database. Figure 12 shows the phase stability diagram (amount of phases vs temperature) obtained from Thermo-Calc calculation with TCFE6 database. Close symbols correspond to 12.5Cr-5Ni steel, while the open symbols correspond to 14.5Cr-5Ni steel. BCC phase stable at lower temperature [<1023 K (750 °C)] is the α -ferrite phase and that stable at higher temperature [>1423 K (1150 °C)] is the delta-ferrite phase. It is observed from this equilibrium phase stability diagram that the stability of delta-ferrite phase extends to much lower temperature [373 K (100 °C) lower] for 14.5Cr-5Ni steel than for 12.5Cr-5Ni steel. Although this diagram does not predict the effect of non-equilibrium cooling on phase stability, one can argue, seeing the equilibrium phase domain, that under non-equilibrium cooling 14.5Cr-5Ni weld metal is likely to have the delta-ferrite at room temperature because temperature range in which austenite phase alone is stable is less by ~ 373 K (100 °C) in this steel than in 12.5Cr-5Ni steel. Hence, during cooling of the weld after solidification, 14.5Cr-5Ni steel spends less time in the

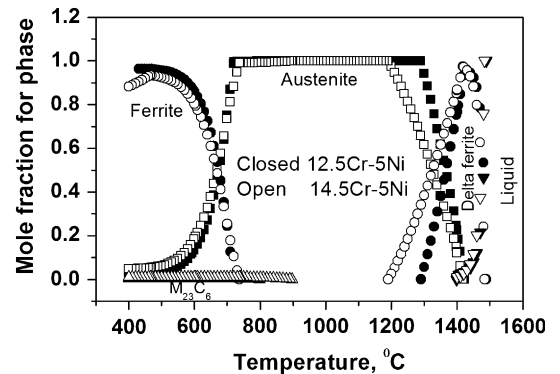


Fig. 12—Phase balance diagram of (a) 12.5Cr-5Ni and (b) 14.5Cr-5Ni weld metals.

temperature range than 12.5Cr-5Ni steel. Hence, it is likely that time is not sufficient for all the delta-ferrite formed at high temperature to transform to austenite. This is in agreement with the observation of delta-ferrite in the microstructure of 14.5Cr-5Ni steel (Figure 2(d)). Further, Figure 12 also shows that the equilibrium amount of $M_{23}C_6$ precipitates present below 1173 K (900 °C) is more (0.01) in 14.5Cr-5Ni alloy than in 12.5Cr-5Ni alloy (<0.001). This is in line with the observation of $M_{23}C_6$ precipitates in the microstructures

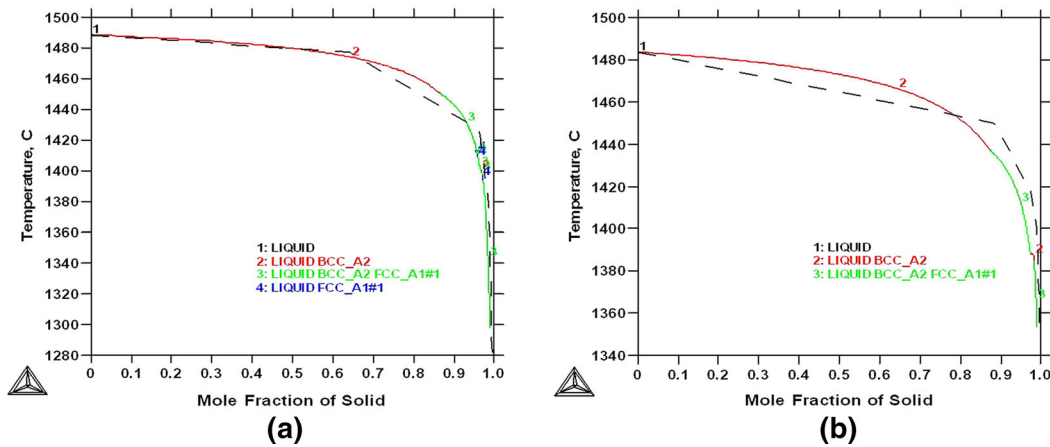


Fig. 13—Scheil solidification simulation results of (a) 12.5Cr-5Ni alloy and (b) 14.5Cr-5Ni alloy.

(Figure 3(h)); these precipitates are more clearly visible in 14.5Cr-5Ni weld metal than in 12.5Cr-5Ni weld metal. The solidification sequence also has been calculated by doing Scheil solidification simulation for both the weld metals. The resulting plots are shown in Figures 13(a) and (b). The solidification sequence observed till the completion of solidification in 12.5Cr-5Ni weld metal is $L \rightarrow L + \delta \rightarrow L + \delta + \gamma \rightarrow L + \gamma$, whereas in 14.5Cr-5Ni weld metal, it is $L \rightarrow L + \delta \rightarrow L + \delta + \gamma$. Delta-ferrite remains during the last stage of solidification for the 14.5Cr-5Ni weld metal. This calculation indicates that the probability of delta-ferrite to be retained at room temperature is high for this alloy, as is found to be the case from microstructure study (Figure 2(d)).

B. Structure–Property Correlation

The observed high hardness value in AW-1 and AW-2 weld metals reported in Table II are due to the formation of fresh lath martensite in both the weld metals. The lower hardness in AW-1 weld metal than AW-2 weld metal is attributed to the fact that low carbon soft martensite is formed in the former. In AW-2 weld, combined effect of high C content and the presence of delta-ferrite, being low in carbon, cause increase in the carbon content in the martensite that causes the high hardness in the as-welded condition. In weld metal of martensitic steels hardness varies from 400 to 450 VHN in the absence of soft phases like austenite and delta-ferrite.^[27] The PWHT at 923 K (650 °C) for 1 hour (1A and 2A) decreased the hardness value due to tempering. With increase in PWHT duration (2 and 4 hours), the hardness value of 1B, 1C, 2B, and 2C specimens remained similar to that of 1A and 2A (Table III). The hardness remained more or less similar is due to the balancing that occurs between tempering of existing lath martensite and fresh martensite (as first stage PWHT is done above A_{c1} temperature) that form during cooling after heat treatment. Hence, morphology of martensite remains similar after these heat treatments and even similar to that observed in as-welded condition (Figures 3(a) and (b)). Although carbon content is more in 14.5Cr-5Ni weld metal than in 12.5Cr-5Ni weld metal,

some carbon has combined with chromium and forms $M_{23}C_6$ carbide at the delta-ferrite/matrix interface which leads to a reduction of carbon and chromium contents in the matrix. This could be the reason for obtaining similar hardness in both the weld metals in different heat-treated conditions. However, the influence of austenite and delta-ferrite in 2A, 2B, and 2C conditions cannot be ruled out. In agreement with hardness, toughness values were similar in AW-1, 1A, 1B, and 1C specimens. The high toughness value of AW-1 is due to the soft low carbon martensite with very small fraction of austenite. Similar results are reported for solutionized 17-4 PH stainless steel which contains low carbon (0.02 wt pct).^[28,29]

Relative decrease in hardness value after second stage heat treatment at lower temperature [873 K (600 °C) for 2 hours], observed in 1D and 2D specimens, is attributed to the combined effect of coarsening of existing tempered martensite (further tempering of already tempered lath martensite) and segregation (austenite stabilizing elements) induced austenite formation and their stability at room temperature. Recently, Tamura *et al.*^[25] reported such coarsening of matrix phase in P91 steel during prolonged tempering at 1023 K (750 °C) for more than 20 hours. Abe *et al.*^[30] reported an increase in lath size caused by the movement of Y-junctions present in 9Cr steel. The Y-junction is a triple point of lath boundaries. The progressive local coalescence of two adjacent lath boundaries near the Y-junction causes the movement of Y-junction. Li^[31] pointed out that the polygonal boundaries that are free from precipitates would be highly mobile under applied stress. In second stage, PWHT carried out herein was very close to A_{c1} temperature, where coarsening cannot be ruled out.

The subsequent increase in duration of PWHT at 873 K (600 °C) for 4 hours increased the hardness value in both the weld metals. The variation in hardness and toughness values is due to change in grain size (Figures 3(d) and (h)) of the material caused by heat treatment in second stage. Recrystallization of austenite phase during prolonged PWHT can refine the grains. The boundary length remains more or less similar during first stage heat treatment. Once the second stage heat treatment at lower temperature is carried out, the

decrease in boundary line density is clearly evident, which is in conformity with the coarser features seen in Figures 3(c) and 6(a). Reduction in boundary length suggests reduction in resistance to deformation and is the reason for the decrease in hardness (Figure 7). Further increase in duration to 4 hours increases the boundary line density which is possible if the grain refinement occurs in the material during heat treatment (as seen from Figures 3(d) and 6(b)) which can result in an increase in hardness. Toughness of a material depends on hardness which indirectly represents the strength and ductility. Figure 14 shows load–displacement plot of 1D and 1E specimens. From the figure, it is evident that the peak load remains similar for both the conditions but the displacement is less for 1D condition compared to 1E condition. It is also shown that the height of the serrations is less in 1D condition compared to 1E condition. Height of the serration is a measure of work-hardening capability of the austenite phase. In both the conditions, the volume fraction of austenite does not vary significantly. Therefore, any change in morphology of austenite which in turn changes the morphology of matrix phase has an influence on toughness. Such changes in morphology are reported by Lee *et al.*^[3] In addition to this, marginal increase in retained austenite may also be attributed to the increase in toughness.^[28,32]

The low toughness of AW-2 weld metal is due to the presence of brittle carbide network at the delta-ferrite/matrix interface, despite the presence of 8 to 10 pct retained austenite in un-tempered lath martensite. Similar carbide network was reported in AISI 403 stainless steel (Cr-0.15C).^[7] Carbon and chromium contents are higher in AW-2 weld metal than AW-1 weld metal. After PWHT at 923 K (650 °C) for 1 hour (Table III), the toughness value of 2A increased to 64 J due to tempering of martensite and the presence of retained austenite. The increase in toughness to 84 J after second stage PWHT at 873 K (600 °C) for 2 hours (2D) and to 100 J after 4 hours (2E) PWHT is attributed to the further tempering of existing lath martensite in addition to increase in volume fraction of retained austenite. The variation in hardness and toughness values with the volume fraction of retained austenite for both the weld metals is plotted in Figure 15(a). From the figure, it is evident that, in 12.5Cr-5.5Ni weld metal,

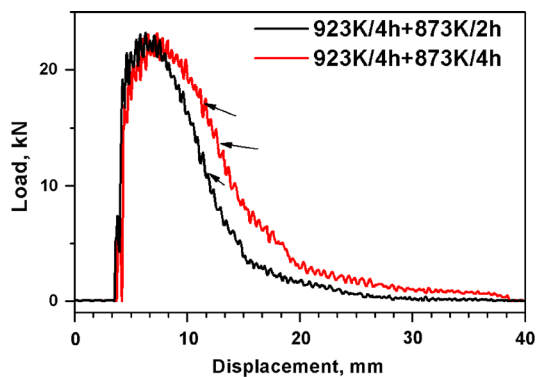


Fig. 14—Load–displacement plots for 1D and 1E conditions.

the impact toughness value reaches a minimum value with the increase in volume fraction of austenite and with further increase in volume fraction of austenite, the impact toughness value increases. At this point, it is necessary to state that such a decrease in toughness with increase in austenite fraction is not expected. But it can be stated that in a soft martensitic material, it is not the volume fraction rather morphology of soft phase has influence. Although direct evidence is not available in this study, fractograph (Figure 9) and boundary line length (Figure 7) support this argument. However, the toughness value of 14.5Cr-5.5Ni weld metal increases continuously during first stage and second stage heat treatments with austenite volume fraction reaching a maximum of 15 pct. The variation of hardness with austenite fraction is similar in both the weld metals except for the high hardness in AW-2 weld metal in the as-welded condition, which, as explained earlier, is due to formation of high C martensite. The variation of full width at half maximum (FWHM) with hardness is shown in Figure 15(b). Both the weld metals show similar decrease in FWHM until the start of second stage heat treatment. Under these conditions, tempering is predominant. This would mean that the strain in the matrix is decreasing or the crystallite size is increasing or a combined effect of both is observed.

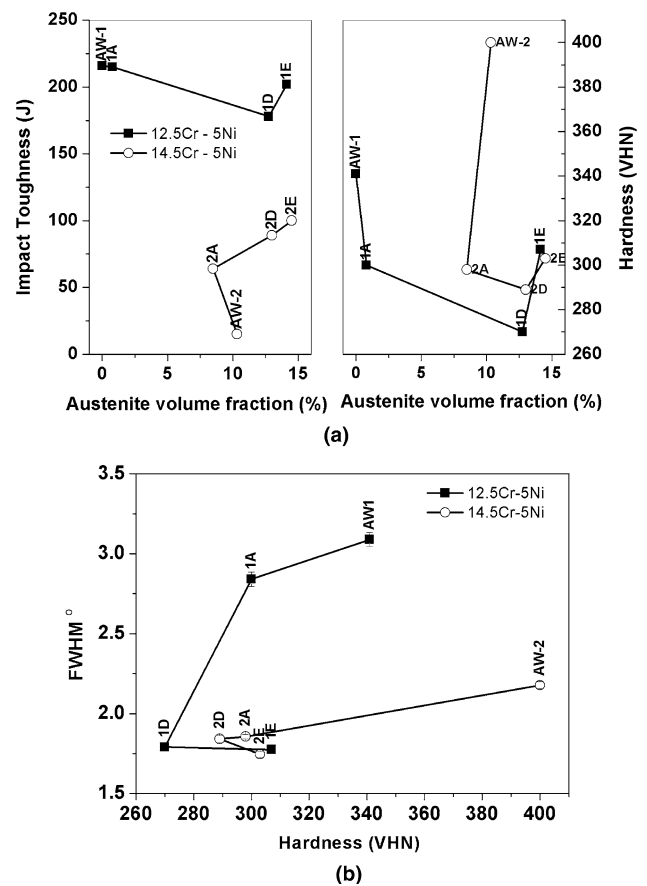


Fig. 15—(a) Variation of impact toughness and hardness with austenite volume fraction in 12.5Cr-5Ni weld metal and (b) Variation of FWHM (211) with hardness of both the weld metals.

C. Influence of Austenite on Properties

As discussed in Section III-E and in Figure 4(b), the bright regions which are rich with austenite stabilizing elements are formed at the end of second stage heat treatment in 12Cr-5Ni weld metal. In 14Cr-5Ni weld metal, austenite stabilizing elements were observed in carbide/matrix interface. Song *et al.*^[10] reported the presence of carbide precipitates in 13Cr-4Ni steel after first stage tempering at 953 K/4 h (680 °C/4 h) and these carbides acted as heterogeneous nucleation sites for austenite during second stage tempering. In order to know the elemental distributions in different phases, these authors used 3D atom probe elemental analysis and observed enrichment of Ni, Mn, and Cr in the austenite. It was mentioned earlier that $M_{23}C_6$ precipitates nucleate at the delta-ferrite/matrix interface during solidification and these precipitates coarsen during subsequent PWHT. Coarsening of these precipitates occurs by diffusion of Cr from the delta-ferrite and matrix phase. As a result, the region close to the precipitate/matrix interface gets enriched with austenite stabilizing elements. Austenite stabilizing elements decrease M_s temperature and hence regions which are enriched with these elements remain as austenite during subsequent cooling to room temperature from the second stage PWHT. Nickel diffusivities at 873 K and 953 K (600 °C and 680 °C) are 2.1×10^{-15} and 3.5×10^{-14} cm²/s, respectively, in iron.^[32] Higher diffusivity at higher PWHT temperature aids in uniform distribution of nickel in the matrix, resulting in high transformation temperature, which in turn results in lesser volume fraction of austenite. On the other hand, at lower temperature, low diffusivity caused significant enrichment of nickel as effective diffusion path reduces. As a result, transformation temperature reduces locally and results in higher volume fraction of austenite at the end of second stage PWHT. This has been reflected as multiple serrations in load–displacement plots shown in Figure 1.

The presence of retained austenite in the weld metal and its variation with composition and heat treatment seem to affect the crack propagation of the weld metal during impact testing. Normally, serrations observed in load–displacement plots (Figure 1) are attributed to the dynamic nature of the experiments, but in the present study, these appear to be linked to the presence of austenite. As volume fraction of austenite was less in single-stage heat-treated 12.5Cr-5Ni weld metal, number and height of the serrations were less in these specimens. But the serrations increased in second stage heat-treated specimens. It is worth noting that the serrations were not pronounced in 14.5Cr-5Ni weld metal in spite of it having higher volume fraction of retained austenite even in as-welded condition. In this alloy, the presence of weak interface between matrix and carbide network (present at the matrix and delta-ferrite interface) dominates over ductile failure in the as-welded and in the first stage heat treatment conditions. However, after second stage heat treatment, the influence of brittle phase reduces as austenite phase nucleates at the precipitate/matrix interface which masks the detrimental effect of brittle phase (weak interface between matrix

and delta-ferrite) leading to lesser serrations. This observation is in agreement with the fractographs shown in Figures 9(a) and (b). From this study, it is clear that austenite nucleates at the precipitate/matrix interface in this class of weld metals which is similar to that observed by others.^[10,19] It is also evident that the presence of retained austenite is not sufficient condition to improve the toughness of weld metal if the delta-ferrite is present in the material.

V. IMPLICATIONS

The present study shows that 14.5Cr-5Ni weld metal has lower toughness than 12.5Cr-5Ni weld metal under different PWHT as well as in the as-welded conditions. This is because of the presence of delta-ferrite in this weld metal. It has been reported by Das *et al.*^[6] that even 12.5Cr-5.5Ni weld metal can have low impact toughness if it contains delta-ferrite. Although Scheil solidification simulation does not predict retention of delta-ferrite in 12Cr-5Ni weld metal during the last stage of solidification, based on our experience with this filler wire, it is understood that the cooling rate is important during welding in deciding the final microstructure. At higher cooling rate, which is experienced during welding of thick components, delta-ferrite to austenite transformation remains incomplete and hence delta-ferrite can be retained in the weld metal. Low toughness in the presence of delta-ferrite (as seen in 14.5Cr-5Ni) is attributed to the formation of a continuous network of carbides along the delta-ferrite matrix interface. Hence, it is emphasized that the proper welding parameters should be adapted to avoid formation of delta-ferrite in welding consumables made of high Cr and Ni martensitic stainless steels. Further studies are necessary on optimisation of welding parameters to minimize the formation of delta-ferrite in this class of welding consumables. Results seem to suggest that attempting to match the composition of the weld metal with that of the base metal may not yield desirable results because weld solidification and high cooling rate experienced for the weld metal has influence on the weld metal microstructure and hence its properties for higher chromium and nickel steel weld metal.

VI. CONCLUSIONS

1. Higher toughness values of 12.5Cr-5Ni weld metal in all conditions as compared to 14.5Cr-5Ni weld metals are attributed to low carbon martensite and the absence of delta-ferrite.
2. The lower toughness in 14.5Cr-5Ni weld metal is due to the high carbon martensite, carbide network at the weaker interface between matrix and delta-ferrite in spite of 10 pct retained austenite in the weld metal.
3. The hardness and toughness remain relatively unchanged in 12.5Cr-5Ni weld metal after first stage PWHT. Toughness improves in 14.5Cr-5Ni weld metal after first stage PWHT and toughness value increased further on second stage PWHT.
4. The changes in toughness after second stage heat treatment in 12.5Cr-5Ni weld metal are discussed

based on changes in microstructural features and volume fraction of austenite. However, the continuous increase in toughness after second stage heat treatment in 14.5Cr-5Ni is due to the tempering and changes in austenite volume fraction.

5. Serrations were observed predominantly in 12.5Cr-5Ni weld metal after two stage PWHT and related to the resistance to crack propagation.

ACKNOWLEDGMENTS

The authors acknowledge support received from the Prof. Indradev Samajdar, IIT Mumbai, India, and National Facility of Texture and OIM—a DST-IRPHA facility at IIT Bombay for carrying out EBSD experiments. The authors would like to thank Shri. S. Arunkumar and Dr. B.P.C. Rao for their support for all the XRD measurements.

REFERENCES

1. P.D. Bilmes, C.L. Llorente, C.M. Mendez, and C.A. Gervasi: *Corros. Sci.*, 2009, vol. 51, pp. 876–81.
2. P.D. Bilmes, M. Solari, and C.L. Llorente: *Mater. Charact.*, 2001, vol. 46, pp. 285–96.
3. S.-J. Lee, Y.-M. Park, and Y.-K. Lee: *Mater. Sci. Eng. A*, 2009, vol. 515, pp. 32–37.
4. P. Wang, S.P. Lu, N.M. Xiao, D.Z. Li, and Y.Y. Li: *Mater. Sci. Eng. A*, 2010, vol. 527, pp. 3210–16.
5. T.G. Gooch: *Weld. J.*, 1995, vol. 74, pp. 213s–23s.
6. C.R. Das, S.K. Albert, A.K. Bhaduri, G. Srinivasan, and V. Ramasubbu: *Sci. Technol. Weld. Join.*, 2008, vol. 13, pp. 159–66.
7. C.H. Hsu and H.Y. Teng, Jr.: *Nucl. Mater.*, 2005, vol. 340, pp. 1–11.
8. J.C. Lippold and D.J. Kotecki: *Welding Metallurgy and Weldability of Stainless Steels*, John Wiley & Sons, Inc., Hoboken, NJ, 2005.
9. J.E. Ramirez: *Weld. J.*, 2007, vol. 86, pp. 125s–34s.
10. Y.Y. Song, D.H. Ping, F.X. Yin, X.Y. Li, and Y.Y. Li: *Mater. Sci. Eng. A*, 2010, vol. 527, pp. 614–18.
11. A.W. Marshall and J.C.M. Farrar: *Weld. World*, 2001, vol. 45, pp. 19–40.
12. M.C. Balmforth and J.C. Lippold: *Weld. Res. Suppl.*, 1998, vol. 77, p. 1s.
13. A.L. Schaeffler: *Met. Prog.*, 1949, vol. 56 (11), pp. 680–80B.
14. J. Onoro: *J. Mater. Process. Technol.*, 2006, vol. 180, pp. 137–42.
15. L. Schäfer: *J. Nucl. Mater.*, 1998, vol. 262, pp. 1336–39.
16. K. Anderko, L. Schafer, and E. Materna-Morris: *J. Nucl. Mater.*, 1991, vols. 179–181, pp. 492–95.
17. F. Abe, M. Igarashi, N. Fujitsuna, K. Kimura, and S. Muneki: *Conference Proceeding Advanced Heat Resistant Steel for Power Generation, San Sebastian, Spain*, University Press, Cambridge, 1998, pp. 84–87.
18. R.J. Castro and J.J. Cadenet: *Welding Metallurgy of Stainless and Heat-Resisting Steels*, Cambridge University Press, London, 1968.
19. S.A. Bashu, K. Singh, and M.S. Rawat: *Mater. Sci. Eng. A*, 1990, vol. 127, pp. 7–15.
20. D. Carrouge, H.K.D.H. Bhadeshia, and P. Woollin: *Sci. Eng. A*, 2010, vol. 527, pp. 3210–16.
21. G. Alkan, D. Chae, and S.-J. Kim: *Mater. Sci. Eng. A*, 2013, vol. 585, pp. 39–46.
22. H. Klug and L.E. Alexander: *X-ray Diffraction Procedures*, 2nd ed., John Wiley and Sons, New York, 1974.
23. <http://www.msm.cam.ac.uk/map/crystal/tar/xrdcalc.tar>. Accessed 3 June 2012.
24. Thermo-Calc Software AB, Stockholm, Sweden.
25. M. Tamura, Y. Haruguchi, M. Yamashtia, Y. Nagaoka, K. Ohinata, K. Ohnishi, H. Ito, K. Shinozuka, and H. Esaka: *ISIJ Int.*, 2006, vol. 46, pp. 1693–1702.
26. D. Carrouge, H.K.D.H. Bhadeshia, and P. Woollin: *Sci. Technol. Weld. Join.*, 2004, vol. 9, pp. 377–89.
27. T.C. Totemeier, J.A. Simpson, and H. Tian: *Mater. Sci. Eng. A*, 2006, vol. 426, pp. 323–31.
28. C.R. Das, H.C. Dey, G. Srinivasan, S.K. Albert, A.K. Bhaduri, and A. Dasgupta: *Sci. Technol. Weld. Join.*, 2006, vol. 11, pp. 502–08.
29. C.R. Das, A.K. Bhaduri, S.K. Albert, and A. Dasgupta: *Int. J. Nucl. Sci. Technol.*, 2009, vol. 4, pp. 355–65.
30. F. Abe: *Mater. Sci. Eng. A*, 2004, vols. 387–389, pp. 565–69.
31. J.C.M. Li: *Acta Metall.*, 1960, vol. 8, pp. 563–73.
32. K. Hirano, M. Cohen, and B.L. Averbach: *Acta. Mater.*, 1961, vol. 9, pp. 440–45.